CANADIAN JOURNAL OF EXPLORATION GEOPHYSICS

VOL. 48, NO. 1 • SPRING 2025

Anisotropic Direct Probabilistic Inversion for unconventional tight reservoirs

Bill Goodway, Raul Cova, Evan Mutual, Adriana Gordon, Irina Berezina, and Scott Leaney

QEYE, CALGARY, CANADA

* CORRESPONDING AUTHOR EMAIL ADDRESS: BG@QEYE-LABS.COM

ABSTRACT

In the application of seismic-based Quantitative Interpretation methods for characterizing unconventional tight reservoir formations, there is a need to improve and, in many cases, correct the standard AVO inversion estimates of key seismic petrophysical parameters (rock properties) that control hydro-frac stimulation. These parameters include the heterogeneity of rock quality (e.g. mineralogy, porosity, TOC, fluid saturation), natural fractures and in-situ stress.

However, subsurface information obtained from standard AVO inversion is often highly ambiguous and nonunique since different lithologies and fluid configurations result in similar elastic responses. This non-uniqueness is an intrinsic characteristic of the inversion problem which can be mitigated by integrating relevant and non-redundant prior geological information into the inversion process. For example, standard inversion techniques are “unaware” of the lithological deposition, bed thickness distributions, anisotropic properties, and petrophysical relationships such as lithofacies, effective porosity, kerogen and fluid fill within the reservoir.

In this paper we show how, under reasonable assumptions, a high-dimensional Bayesian inference problem enables the application of a general and flexible probabilistic framework for rigorous propagation of uncertainties. This is accomplished through using a prior facies model built using geological knowledge and rock physics measurements from multiple domains such as logs, core, petrophysics, depositional environment and associated vertical transverse isotropic layering effects; that can be easily integrated into a probabilistic inversion method termed VTI Direct Probabilistic Inversion.

INTRODUCTION

Decision-making for exploration and development well placement and risk analysis using seismic reservoir characterization requires an increasing degree of assessment of the uncertainties associated with seismic Quantitative Interpretation (QI) predictions. Bayesian inference provides a framework where these issues can be addressed (Larsen et al 2006). However, in its standard formulation, and given the size of typical seismic volumes, Bayesian inference might be computationally prohibitive. In this paper we show how, under reasonable

assumptions, a high-dimensional Bayesian inference problem can be reduced to several local low-dimensional inference problems, reducing the computational cost of this solution. This enables the application of a general and flexible probabilistic framework for rigorous propagation of uncertainties where prior knowledge from multiple domains can be integrated within a Direct Probabilistic Inversion (DPI) method.

Such prior information is readily available from logs, core and geological studies that provide a model for specific ranges of elastic properties for target zone facies, average thicknesses and their petrophysical variation, stratigraphic position within a formation, as well as the presence of gas, oil, or kerogen content. By defining a set of rules based on this information it is possible to dramatically reduce the solution space (Hansen et al 2018). However, in conventional deterministic seismic inversion algorithms all this prior information is difficult to integrate. Moreover, the correct propagation of uncertainties through these inversion methods is not possible. These additional prior constraints of thickness, ordering, etc. can also help resolve units that are below seismic resolution due to weak reflectivity contrasts.

In particular, the case study will illustrate how DPI can leverage this extra information to significantly improve the resolution of near invisible low impedance contrast zones such as the Montney. Not only does this lead to a better interpretation of the low impedance contrast intervals but also helps mitigate the ambiguity in isolating the target reservoir properties, that are difficult or impossible to differentiate in deterministic inversion.

We tested Anisotropic DPI in Canada on the Montney formation. The Montney formation is a large, active, resource play in North America, with a potential of up to 449 trillion cubic feet (Tcf) of natural gas (Mutual et al., 2024a). It is a thick formation, comprised of numerous silts and shales with varying reservoir properties. Extensive drilling activities and associated data collection within the Montney formation provide definition for the facies, depositional style, and rock properties of its major units (Mutual et al., 2024a). Thinly bedded shale units within the Montney can be described as having VTI (Vertically Transverse Isotropic, see Thomsen, 1986) anisotropy, and may overlay other tight silt, sand and shale units.

The evidence we present for the value of the anisotropic extension to DPI begins with a high-level theoretical description of the DPI process, followed by a simple theoretical VTI modeling exercise. This shows that a VTI effect can create a false positive in AVO inversion (Blangy, 1994). Next, we discuss how VTI effects and other rock physics modeling fit into the DPI process. Finally, we demonstrate results on simple synthetic models, and subsequently on actual 3D seismic data with well control.

THEORY

Direct Probabilistic Inversion (DPI) workflow accounting for anisotropic VTI effects

The general underlying DPI approach (Figure 1) consists of a one-step inversion process based on the Bayesian probabilistic formulation introduced by Jullum and Kolbjørnsen (2016), based on earlier work by Buland and More (2003). This method honours multi-domain inputs and

assumptions, ensuring the confidence range in these inputs. A key feature of DPI is that the geological framework of prior information can be encoded and combined with seismic AVO modeling to provide reliable results. This geological framework might include geological and petrophysical relationships such as encasing VTI shale facies, lithofacies with effective fracture porosity, kerogen and fluid-fill in non-equant porosity, elastic property ranges and intra property and distance correlations for each facies. The prior information including several elastic property relationship models can be broad and plausible but also very strict depending on the level of available knowledge. By incorporating spatial information, DPI optimizes the propagation of uncertainty and addresses the non-uniqueness of the problem by providing probability distributions. Under certain conditions, this reduction in the solutions space allows DPI to extract features beneath the seismic resolution limit.

The result of the DPI process is a probability volume for each of the defined geological facies and anisotropic petrophysical parameters, including VTI layering, natural fractures and in-situ stress. Furthermore, many other properties can be derived from having the probability for each facies. For example, all the facies' elastic parameter probabilities can be combined using the full AVO signal and the geological information into the most likely facies and corresponding probability. This will be discussed further in the next two subsections. Finally, by integrating all these probabilities, a volume of high-resolution sub-tuning intervals is produced.

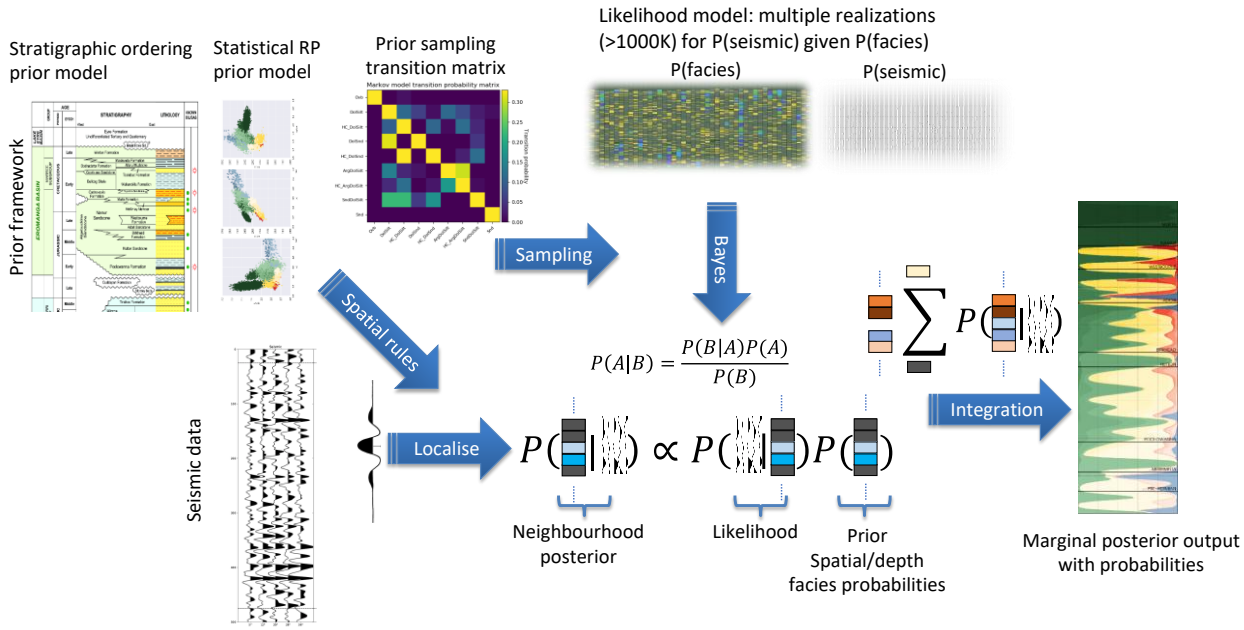

Figure 1: Schematic workflow for the Bayesian inference probabilistic QI DPI method (Adapted from Goodway et al., 2021)

DPI method

Motivated by the above observations, the problem can be formulated as a Bayesian inference problem (Tarantola, 2005).

$$s(\boldsymbol{m}) = cr(\boldsymbol{m})L(\boldsymbol{d}_{obs} - g(\boldsymbol{m})) \quad (1)$$

where $\boldsymbol{m}$ represents the subsurface model parameter configuration. In this context, information about $\boldsymbol{m}$ is described by a probability density function (pdf). In the initial state of the inference, that is prior to the seismic data experiment the information is described by the prior pdf, r. This is updated with the information from the seismic AVO data via the likelihood function L, which measures, in terms of probability, the misfit between forward modelled $g(\boldsymbol{m})$ and the measured seismic AVO data, c is a normalizing constant, and the posterior pdf, s, constitutes the updated state of inference of our subsurface model parameters. Generally, the posterior pdf cannot be evaluated analytically, and hence one must resort to a sampling-based approximation.

For the current problem, surfaces are defined as transitions from subsets of facies, and hence the model parameters, $g(\boldsymbol{m})$, constitute a seismic grid of categorical variables. The prior pdf will be defined by a set of rules for sampling from it, as this is much more general and flexible compared to specifying a closed form of it. The likelihood, L contains, in addition to a seismic noise model, the combination of a statistical rock physics model from facies to elastic property domain, and a seismic convolutional AVO forward model from elastic properties to seismic angle-stack domain. As such, the solution to this problem can be considered a direct or one-step inversion for facies using seismic AVO data.

Markov Chain Monte Carlo (MCMC) sampling methods (Tarantola, 2005) can provide an ensemble of samples, which will converge to the posterior pdf no matter how complex the prior pdf and likelihood function are. However, efficiency is problem dependent and may be difficult to achieve. In addition, the required sampling density in a high-dimensional model space (such as a standard sized seismic volume) means that these methods in general are computationally demanding and time consuming.

For limited compute power and time, several approximations can be made in the context of seismic AVO data and rock physics to make the inference problem computationally feasible. Surfaces of interfaces, defined as facies transitions, are (vertically) of short range or local by nature, and hence the point-wise marginal posterior or the joint posterior in a small volume are much more relevant compared to the long-range correlations of the joint posterior distribution. Additionally, at a given point in the seismic grid, the rock physics model response of a facies can be assumed localized to a small region at and around the point, and the associated seismic convolutional response is limited to a wavelet length above and below the point thus ignoring wave propagation effects outside convolutional modelling of primary reflections. If the prior information is also limited to short range correlations, the high-dimensional inference problem can be split into several low-dimensional problems, which can be approximately resolved by a weighted Monte Carlo method (for more details see Jullum and Kolbjørnsen, 2016). The conceptual outline is:

1. Sample a large number *N* of local region sized facies realizations from the prior pdf.
2. Set up the local likelihood approximate function for each facies sample.
3. At a given point, $\mathbf{p}$, in the seismic grid, extract the observed seismic AVO data, $\boldsymbol{d}_{obs}$, $\mathbf{p}$ in a local region with $\mathbf{p}$ as center.

4. For each facies sample, the local likelihood function with $\boldsymbol{d}_{obs}$, $\mathbf{p}$ as input is evaluated and provides a weight, $v_{\mathbf{p}}$.
5. Normalize the weights, $v_{\mathbf{p}}$, yielding normalized weights, $w_{\mathbf{p}}$.
6. For each facies sample, identify the center value, $f_{\mathbf{p}}$ and pair it with $w_{\mathbf{p}}$.

Steps 3 to 6 are iterated through all the observed seismic data. At a given point in the seismic grid, the sum of the normalized weights for a given facies value approximates the marginal posterior distribution. The accuracy and the computational cost of the method depend on N and the size of the local region around the point, $\mathbf{p}$. Using the estimated posterior marginal pdf and prior spatial information, if available, marginal posterior probabilities can readily be obtained.

Anisotropic extension of DPI

The preceding section describes the DPI inversion process, but the challenges presented by unconventional tight silt shale encased reservoirs often require the use of a more complex treatment to model anisotropic AVO responses, leading to extended VTI DPI.

To implement an anisotropic extension to DPI, we use Ruger's AVO approximation for VTI media (Rüger 1997) as the forward modeling operator to compute the likelihood function in DPI. The benefits of this approach are two-fold. First, it expands the model space from three (AI, V_P/V_S, density) to five elastic parameters, which now includes the two weak anisotropy Thomsen parameters, δ and ε (Thomsen 1986). This expansion provides an opportunity for resolving elastic ambiguities that might not be resolved by using only three isotropic parameters. Secondly, the use of a more complex AVO approximation that accounts for anisotropic effects helps to avoid the misinterpretation of hydrocarbon-related AVO signatures, which might result from the false positive effect of overlaying anisotropic shales above water-saturated sands (Blangy, 1994). The same idea can be extended to unconventional reservoirs where the same incorrect signature can be misinterpreted as a false positive increase in brittleness if the anisotropy of the overlaying shale is not accounted for during the inversion process.

The effect of an unaccounted VTI shale is illustrated by the model in Figures 2 through 4. Figure 2a shows a simple Montney-like model with a VTI layered shale overlaying a tight gas shale. Figure 2b shows the velocity responses with angle within the VTI shale, which is dominated by the V_P increase with angle. Figure 3 shows how the model of the observed VTI AVO response is incorrectly fitted by an isotropic AVO curve thereby compounding the overlying shale's false positive effects with the estimate of the underlying tight gas elastic properties. As shown in the LambdaRho ($\lambda\rho$) vs MuRho ($\mu\rho$) crossplot in Figure 4 (Goodway et al., 2006), this leads to an inaccurate brittleness estimate for V_P/V_{SV} with a near constant AI, a decreasing Poisson's ratio, and an increasing Young's modulus – results that arise from using standard deterministic isotropic AVO inversion. In Figure 4 the standard transform form P-impedance (AI) to Shear impedance (SI) is given as (Goodway, 2001)

$$\lambda\rho = AI^2 - 2SI^2, \text{ and} \tag{2}$$

$$\mu\rho = SI^2 \tag{3}$$

a)

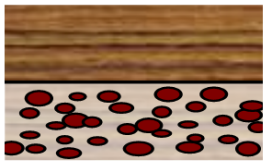

	V_P (m/s)	V_S (m/s)	Rho (g/cm^3)	ε	δ
VTI shale	3797	1864	2.66	0.12	0.1
Tight gas shale	4233	2544	2.55	0	0

b)

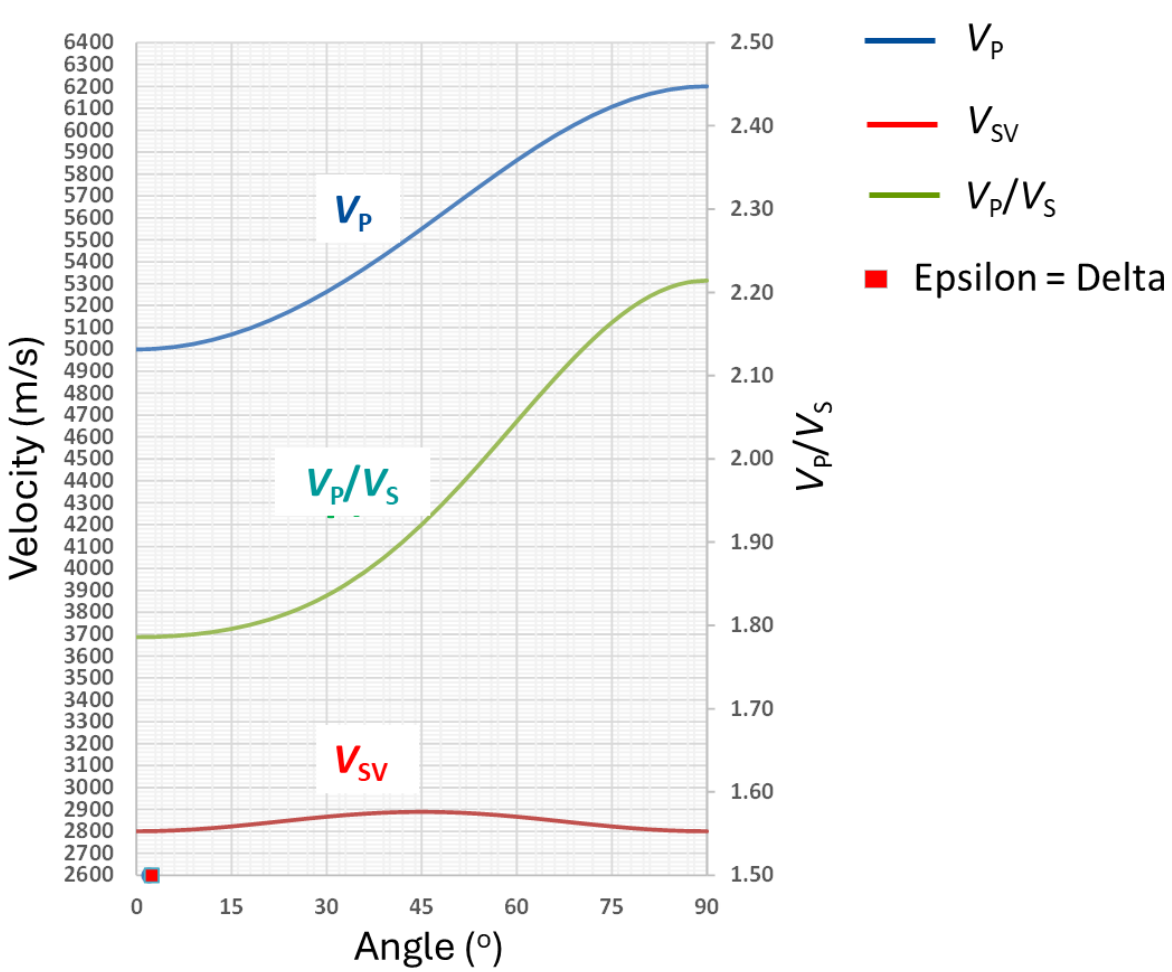

Figure 2: (a) Parameters used in model of VTI shale overlying tight gas shale reservoir. (b) VTI V_P/V_S increase (from V_P and V_{SV}) with angle of incidence in overlying shale layer. VTI V_P/V_S increase with angle in the overlying layer produces a relative V_P/V_S decrease for constant AI in the underlying layer of quartz-rich tight gas shale reservoir.

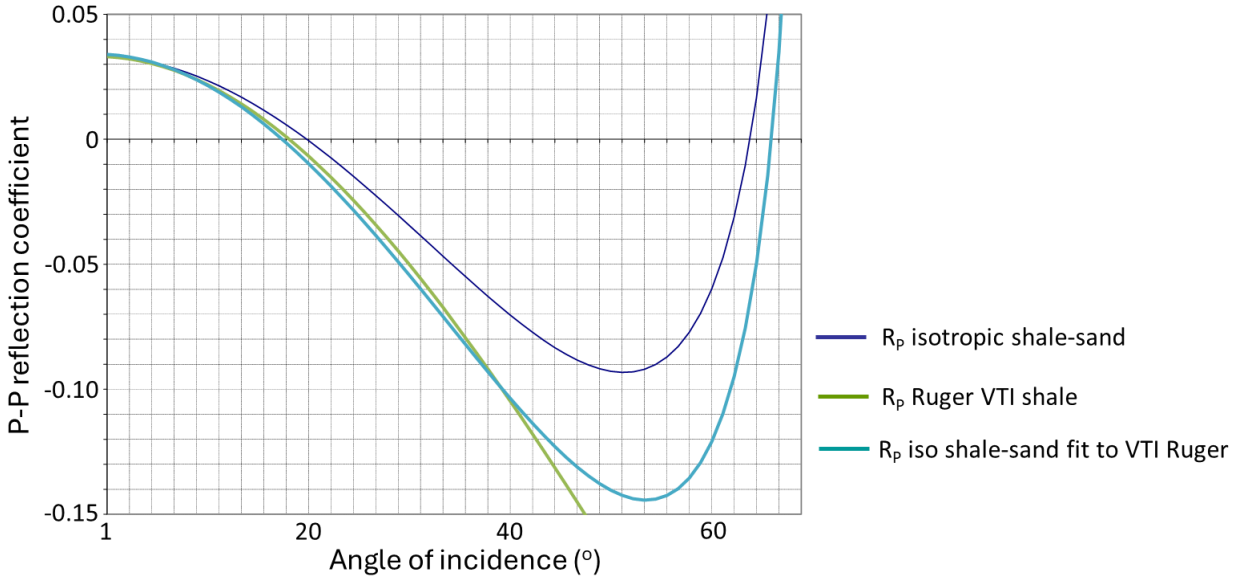

Figure 3: P-P reflectivity versus angle of incidence using V_P/V_S Rho input from Aki-Richard's approximation, VTI Ruger AVO and Thomsen VTI shale V_P/V_S. Observed VTI Ruger AVO curve fitted with an isotropic AVO curve showing the false positive effects of overlying shale VTI.

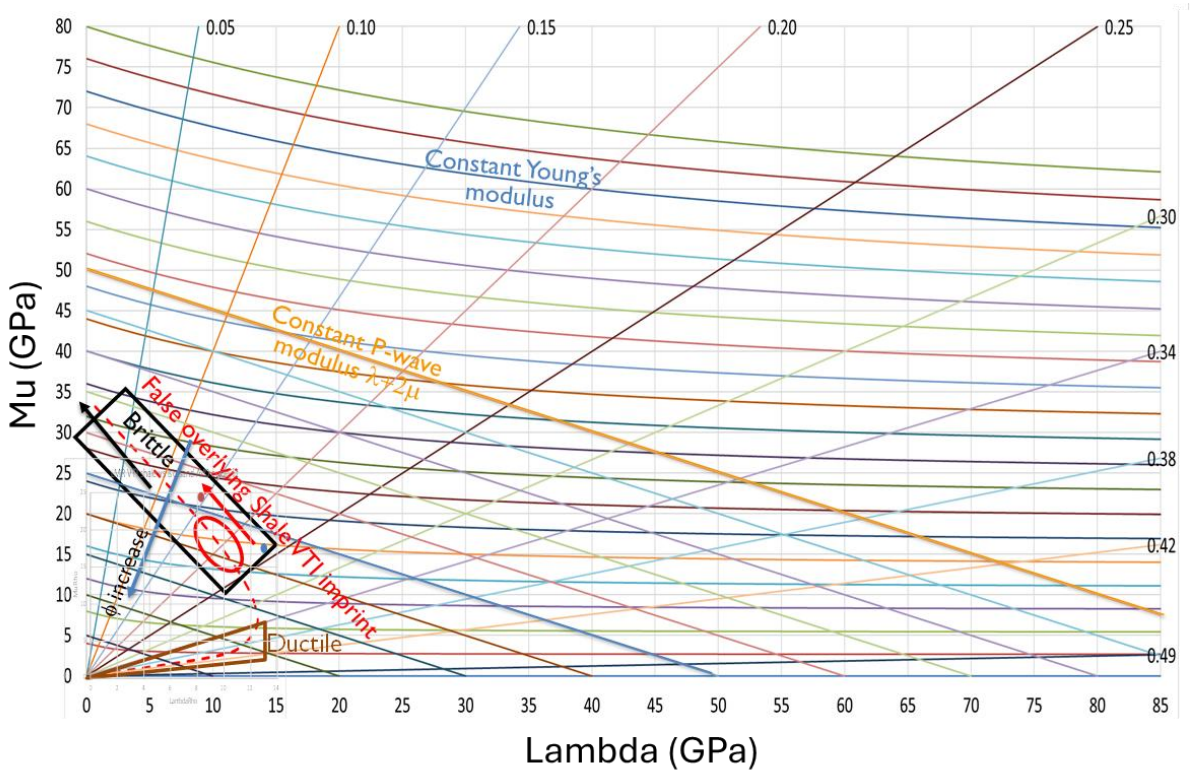

Figure 4: Crossplot for Lambda versus Mu for well data with an overlay of lines of constant Young's modulus (curved), Poisson's ratio (radial), P-wave modulus (sloping) with Grigg-Barnett brittleness trend (dashed). The effects of overlying VTI shale imprint on deterministic AVO guarantees a false positive brittleness trend (Grigg, 2004) in the underlying tight gas shale reservoir target. Compare trends (black-red arrows and red dashed line) for "Brittle" and "False overlying Shale VTI imprint".

Statistical rock physics theory and facies modeling

To prevent these VTI shale effects from becoming a source of error in the inversion, the effects must be included in the analysis. The need to include this complexity into the prior information used in the DPI method from Figure 1 extends to all other relevant lithologic, stress and fluid variables that are expected within the area. Only by doing so can the non-uniqueness of the AVO inversion be addressed. Standard inversion techniques, by contrast, are “unaware” of the lithological deposition, bed thickness distributions and petrophysical relationships such lithofacies, effective fracture porosity, kerogen and fluid fill in non-equant porosity within the zone of interest as shown schematically in the following Figures 5, 6, and 7.

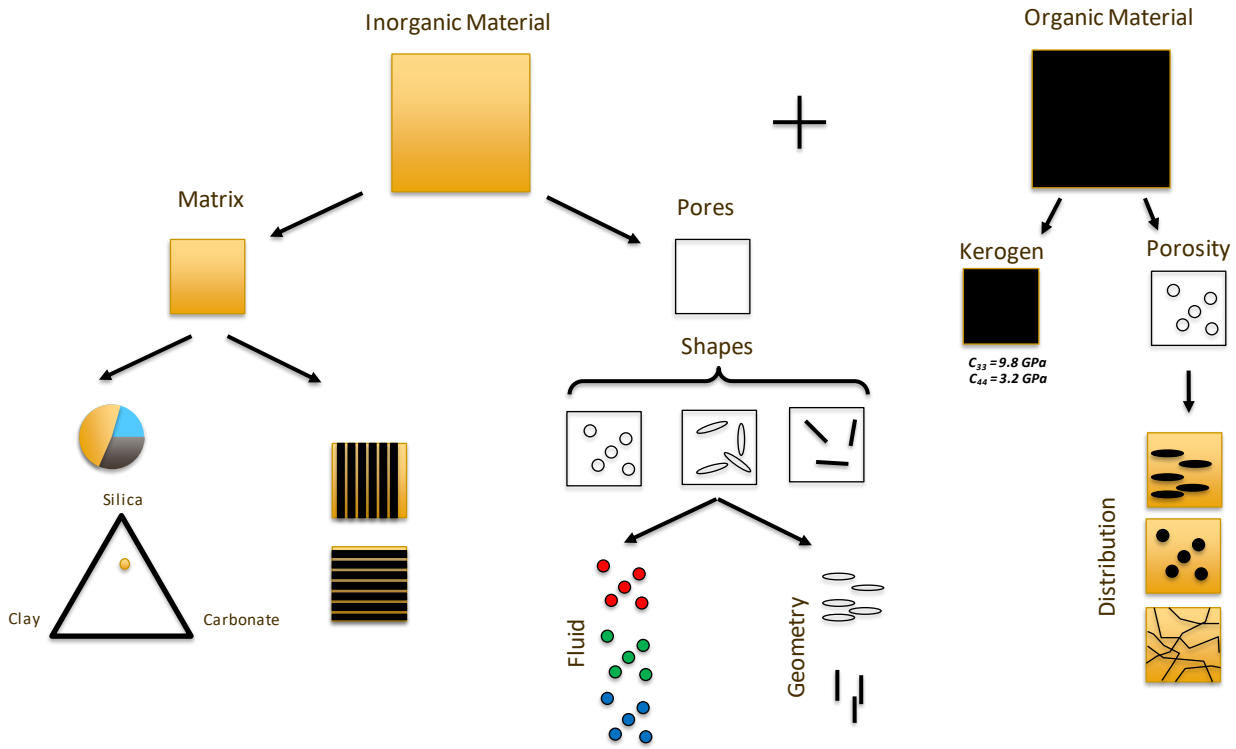

Figure 5: Complex hierarchy of unconventional rock physics classification for model-based relationships. (Adapted from Goodway et al., 2021)

In Figure 7, the anisotropic LMR crossplot is plotted as $c_{13}(c\lambda_{13})and\ c_{44}(c\lambda_{44}weak)$ components of the stiffness tensor. The coloured dots represent the elastic parameters from log-based gas shale zone colour-coded by volume of TOC. The black dots are the samples that correspond to a narrow range of quartz content (47.5 – 52.5%). The blue line joining the dots is the intrinsic VTI anisotropic trend line for this specific mineral quantity-each white dot represents a 10% increase in TOC. The blue line with square dots accounts for the presence of cracks and helps explain the scatter seen in the crossplot.

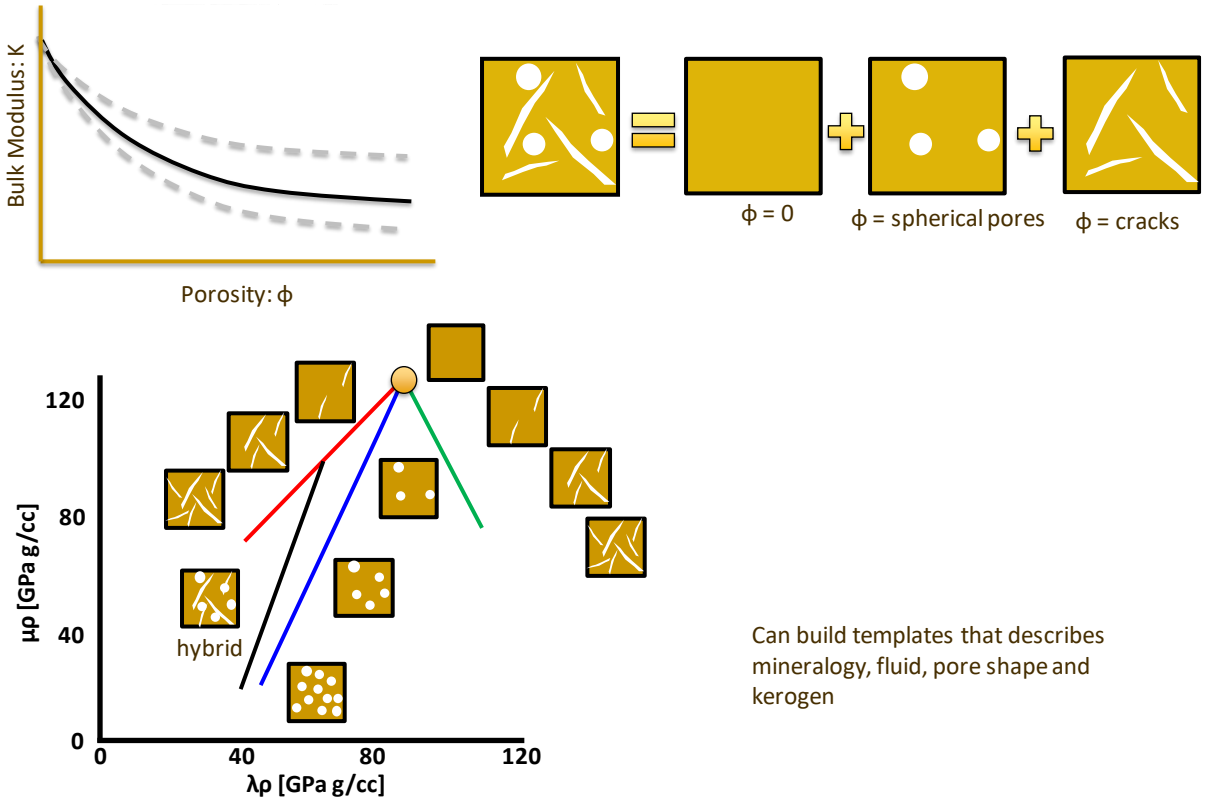

Figure 6: Lambda-Rho versus Mu-Rho crossplot of elastic property models of rock physics that provide prior information templates describing mineralogy, fluid, pore shape and kerogen. (Adapted from Figures 2 and 3 from Perez, 2013)

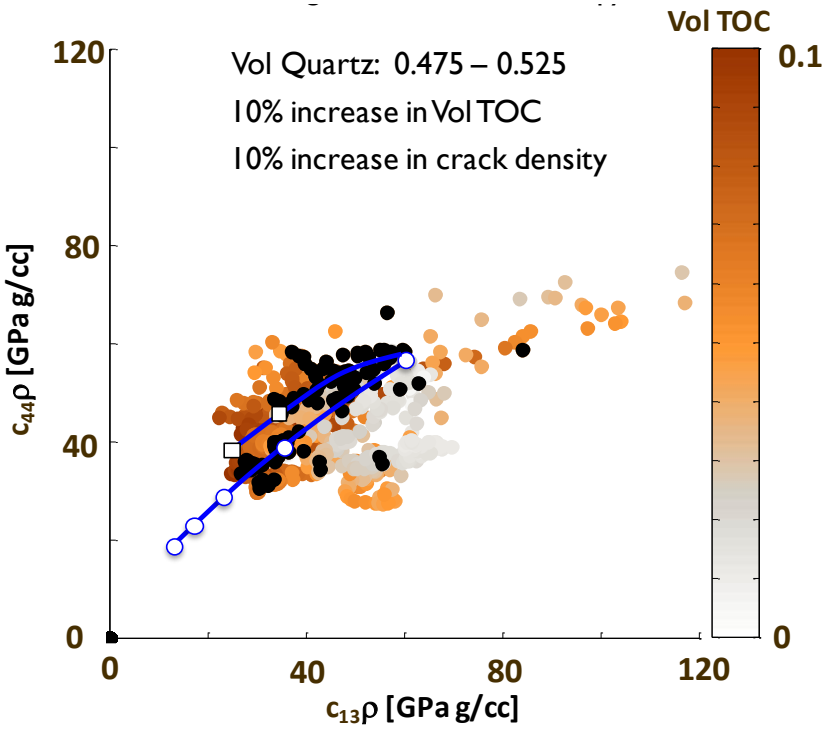

Figure 7: Lambda-Rho versus Mu-Rho crossplot template illustrates the combined rock physics model, accounting for both isotropic and anisotropic effects. These additional effects introduce ambiguity in the elastic parameters, leading to scatter in the model template crossplot due to their overprinting. (Adapted from Figure 2 of Perez, 2015)

The additional information required for effective DPI is readily available from sonic scanner logs, core data and geological studies. These sources provide a model for specific ranges of elastic properties for target zone facies, average thickness and their petrophysical variation, stratigraphic position within a formation, as well as the presence of gas, oil, or kerogen content. This high-level prior information for DPI is carried in facies index logs for multiple wells.

However, we usually face a problem in facies identification and analysis for index logs. When we use the term facies, we do not necessarily mean grouping of rocks only by lithology type, but also by some other property like porosity, or a set of properties like porosity and fluid type. The choice of facies is problem dependent. For facies in unconventional formations, we may also consider defining facies by differences in pore space geometry like round pores and fractures or facies characterized by overpressure thus having different elastic responses (see Figures 5, 6 and 7). Ideally the defined facies should be both geologically and statistically significant so that we have reliable statistics. Generally, classification methods are applied to group the target rocks in facies based on the measured data and vary from simple petrophysical cut-offs to clustering, such as K-nearest neighbors or K-means, to more advanced algorithms such as pattern recognition and algorithms using neural networks and classification trees.

Given the facies index logs, a facies Markov transition probability matrix is generated, and together with a thickness distribution function, a geological sequence realization may be produced. Usually a facies interpretation is provided, which may come from borehole image log interpretation and / or petrophysical cut-offs. If a facies interpretation is not available, we can generate one automatically using any one of a myriad of ML techniques. As an example, in Figure 8 we show a robust k-means algorithm with Monte Carlo initialization applied to Montney elastic logs including a sonic-derived VTI log. Prior to clustering, all logs were normalized to have a median value of 1.

When available the facies index logs are defined by elastic anisotropic (VTI) properties: V_P, V_S, ρ, δ and ε. These logs come from sonic and density logs, database information and rock physics. Sonic-scale anisotropy is utilized, being obtained from advanced sonic waveform processing. In a single well these data provide only three VTI moduli (C33, C55, C66); the two missing moduli (C11 and C13) are obtained by incorporating core database information and rock physics using a Bayesian framework.

Ideally, sonic-scale anisotropy information would be derived from a multi-well / multi-angle inversion of sonic slowness measurements acquired through the same formation. This approach can provide log-scale, complete tilted transversely isotropic (TTI) tensors but such data are rarely available in practice, so other approaches are needed. A limited transversely isotropic (TI) tensor can be measured from sonic logs in a single well. If the well is deviated, crossed-dipole shear logs can be oriented to obtain shear logs corresponding to qSv and Sh (normal and parallel to bedding, respectively). The Stoneley mode can also be processed to obtain the Sh modulus (C66) and hence the shear VTI parameter, gamma. The C66 estimate is generally reliable for low permeability formations but porous sandstone formations can cause negative shear VTI due to the impact of pore fluid mobility on the Stoneley wave. It is not widely known that negative anisotropy in sandstones is expected due to stress sensitivity as in a

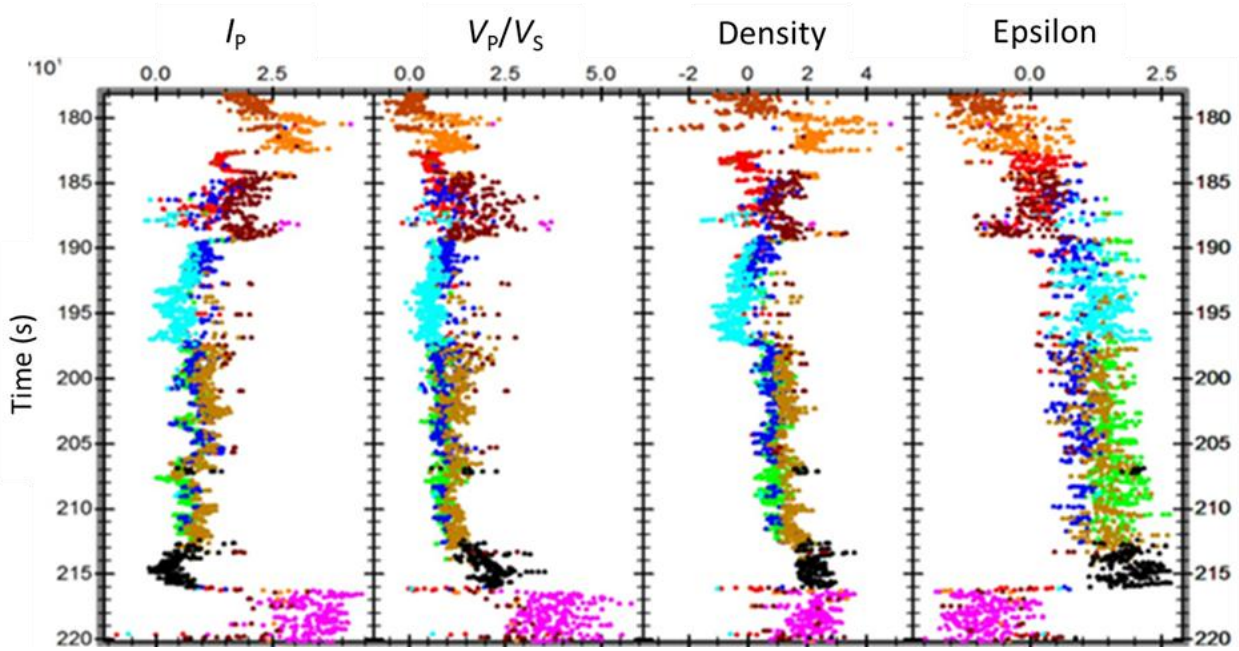

Figure 8: Automatic facies classification over the Montney using four (normalized) elastic logs (Ip, V_P/V_S, density, epsilon). In this example ten facies have been classified. (Adapted from Leaney and Sayers, 2024)

normal faulting regime vertical is the largest effective stress direction. Thus, in addition to anisotropy in clay-rich formations, we incorporate recently developed rock physics modelling in the sonic tensor completion algorithm to include negative anisotropy in sandstone formations. This results in an increased contrast in δ and ε with respect to bounding shales. Given VTI logs (Figure 9a), the facies index allows means and covariance matrix for density and anisotropic parameters to be computed for each facies. These form part of the statistical parameter set for geological sequence realizations in the probabilistic AVA inversion. Away from wells with sonic anisotropy measurements we can use petrophysical correlations. Deviated wells with legacy sonic logs require angle-dependent corrections for anisotropic effects. Where advanced sonic processing is not available, rock physics modelling based on petrophysical properties (e.g. Vclay, PHIT) is used to predict anisotropy. Isotropy is never the most likely scenario, so some prediction of anisotropy is always recommended given that the impact of VTI can be significant on the seismic AVA (amplitude versus angle) response. This is clearly illustrated in the synthetic angle gather comparison (generated from upscaled VTI logs) as seen to the bottom right of Figure 8b.

Defining a set of prior rules based on facies information as in Figure 9a significantly reduces the solution space. In contrast, conventional deterministic seismic inversion algorithms struggle, or are often unable to integrate or incorporate this level of detailed information. Moreover, the traditional approaches do not allow for proper uncertainty propagation, limiting their ability to quantify confidence in the inversion results.

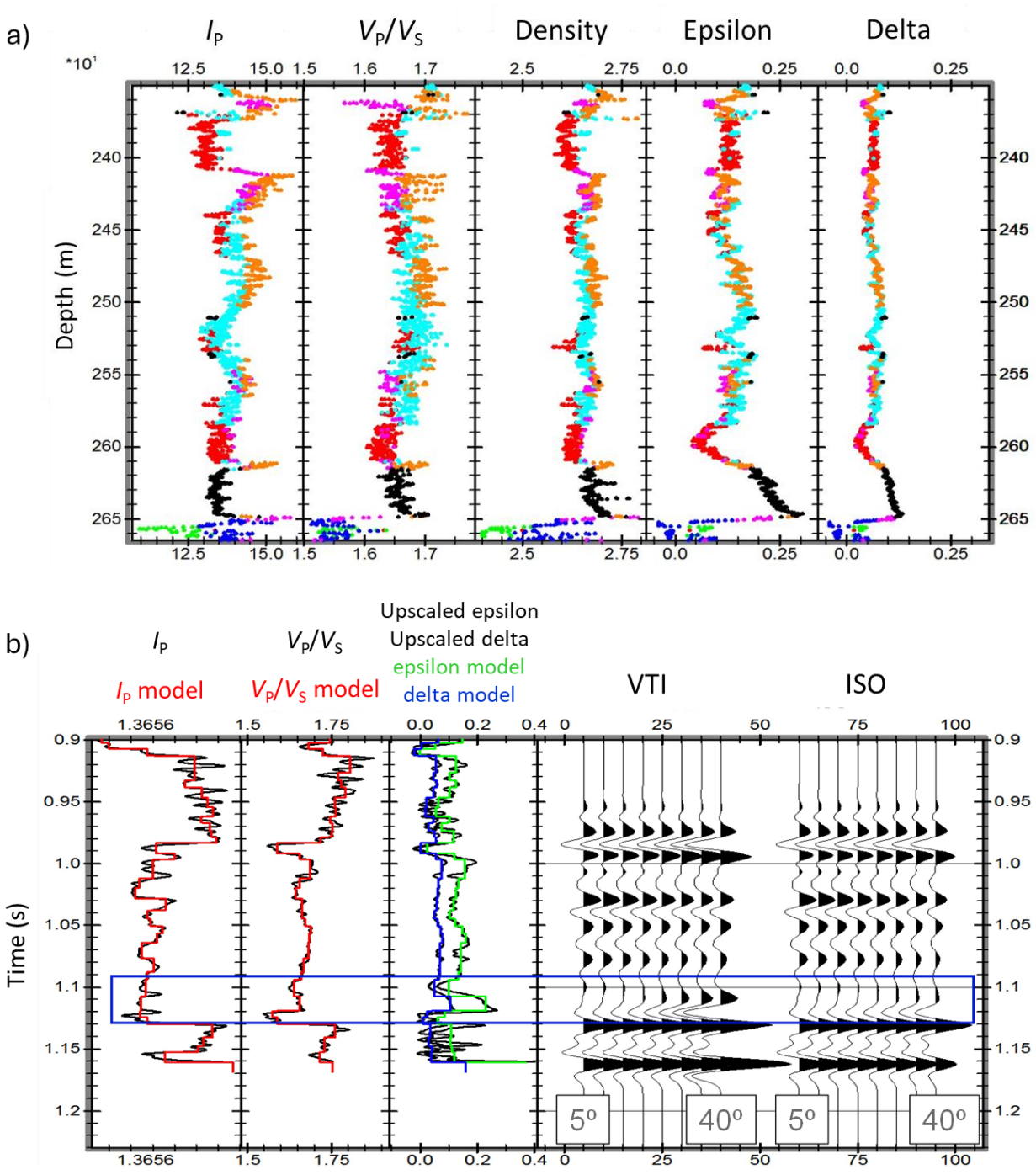

Figure 9: (a) VTI logs (Ip, V_P/V_S, density, epsilon and delta) coloured by facies over a section of the Montney. The facies form the anisotropic priors. (b) Comparison of VTI to isotropic (ISO) AVA synthetics generated from elastic VTI logs Ip, V_P/V_S, epsilon and delta, highlighted by the box over the base of a section of the Montney. (Adapted from Leaney and Sayers, 2024)

RESULTS

Montney example VTI DPI proof-of-concept log synthetic model

Demonstrating the anisotropic DPI method on the Montney Formation begins with a synthetic model, and analysis of the rock properties and facies, as shown in Figure 10. Figure 10a shows the facies model, elastic properties, Thomsen parameters (d, e) and synthetic seismic angle stacks to evaluate the DPI performance. This model was constructed based on a facies log derived from the interpretation of petrophysical and core data. Notice that the upper half of the model is dominated by the interlayering of dolomitic siltstones and dolosandstones, with the dolomitic siltstones showing larger thicknesses. The lower half of the model shows a series of argillaceous dolosiltstones interlayered with dolomitic siltstones. In contrast to the upper half the proportion/thicknesses of the dolomitic siltstones are smaller in the lower half. Figure 9b, depicts the distribution of the elastic properties for each facies in all the possible combinations of the five elastic parameters used in the probabilistic inversion. All the elastic properties values, including the anisotropy parameters, were measured or modelled by well logs. In the AI and V_P/V_S spaces all the facies seem to occupy similar regions. Only when the weak anisotropy parameters are considered, does a clear separation between the underburden facies and others become evident. Additionally, combining V_P/V_S and either δ or ε seems to provide a better separation of the dolosandstones and the argillaceous dolosiltstones. Notice that the dolomitic siltstone remains undifferentiated regardless of the analysis space.

In Figure 10b, one can make a few observations. For example, the **Ovb** and **Und** facies are better separated using Thomsen's parameters, the **DLSS** facies is discriminated by V_P/V_S and density from the **ArgDLSilt,** but it remains partially overlapping with the **DLSilt** in all domains, and the **DLSilt** and **ArgDLSilt** facies are partially overlapping in all domains.

The final component needed for DPI is to encode the geological framework of prior information (see flow chart in Figure 1). As mentioned, this framework includes geological and petrophysical relationships such as encasing VTI shale facies, lithofacies with effective fracture porosity, kerogen and elastic property ranges with intra property and distance correlations for each facies. This prior information is mathematically encoded using the facies transition probabilities with the transition matrix as shown in Figure 10c.

Similarly, in Figure 10c, the **Ovb** facies preferentially transition into the **DLSilt** facies, there is almost equal probability that the **DLSilt** facies transition into a **DLSS** or **ArgDLSilt** facies, the **DLSS** facies preferentially transition into the **DLSilt** facies, and the **ArgDLSilt** facies preferentially transition into the **DLSilt** facies.

CANADIAN JOURNAL OF EXPLORATION GEOPHYSICS

VOL. 48, NO. 1 • SPRING 2025

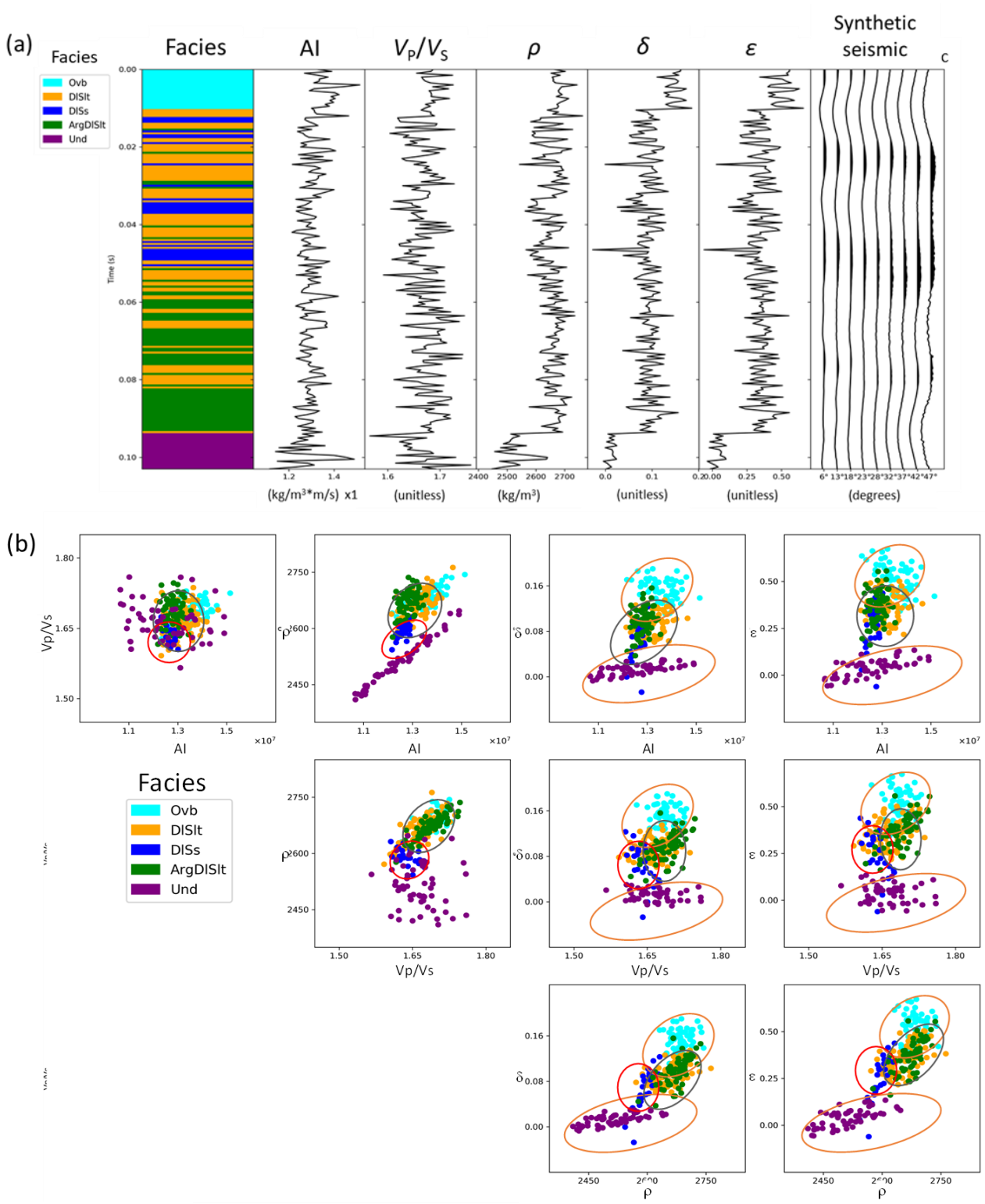

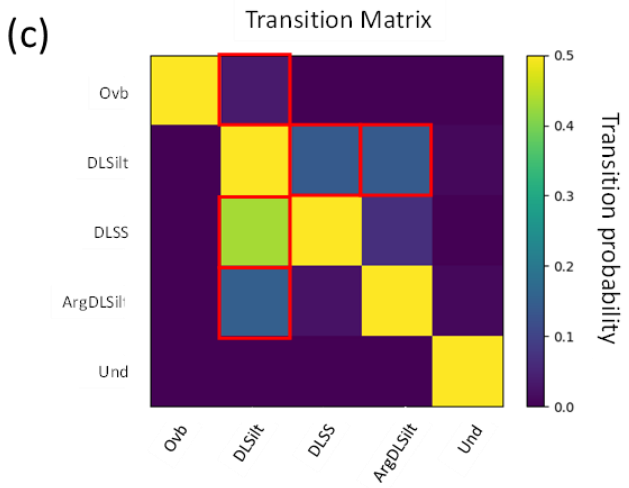

Figure10: (a) 1D facies model, log tracks and forward synthetic gather from Montney well. (b) Crossplots of isotropic elastic parameters (AI, V_P/V_S, ρ) and weak anisotropic Thomsen parameters (δ or ε) from each facies. (c) Facies transition probability matrix.

Montney example VTI DPI proof-of-concept log data model results

Figures 11a, to 11c, illustrate the proof-of-concept results of isotropic and VTI probabilistic inversions for the preceding Montney log data example of Figure 10. Eight synthetic angle-stacked traces between 5° and 36°, were computed using Ruger's VTI approximation based on the available log data shown in the leftmost panels of each figure and same as the rightmost panel of Figure 9a.

In all three figures, the middle panel (colour-coded by facies) is divided into sub-panels, namely: smooth prior facies model (far left) posterior full probability range output, most-probable facies, and finally the observed log facies. In the top right corner, each figure includes a confusion matrix, showing the predicted posterior facies (y-axis) vs the observed facies (x-axis), which enables an assessment of the accuracy of prediction accuracy. The bottom right panels show AI, V_P/V_S and ρ respectively and Thomsen d and e, in Figure 9b where the red tracks represent true log values, and the black overlays represent the mean posterior estimates. The gray bounds indicate two standard deviations.

The prior probabilities for each facies in the leftmost middle panels for the dolomitic siltstone and the argillaceous dolosiltstones are the same with a value of 0.45. While the prior probability for the dolosandstones was fixed at 0.1. These probabilities approximate the proportion of each of those facies within the target window and are tapered down as they approach the expected location of the transition from the overburden to the Montney zone of interest and to the underburden.

In this proof-of-concept test, Figure 11a shows the results of applying isotropic DPI to a VTI synthetic angle gather input (track 1). In the middle panel tracks 3 and 4, the posterior output and most probable facies do not accurately resolve the observed facies with a prediction accuracy of only 47%. This low accuracy is also captured visually in the confusion matrix of the predicted posterior output (y-axis) vs the observed facies (x-axis), having several high probabilities off the 1:1 diagonal. However, in the lower right tracks for AI, the black prediction overlay on the observed red log track shows a good match as the VTI effects only progressively

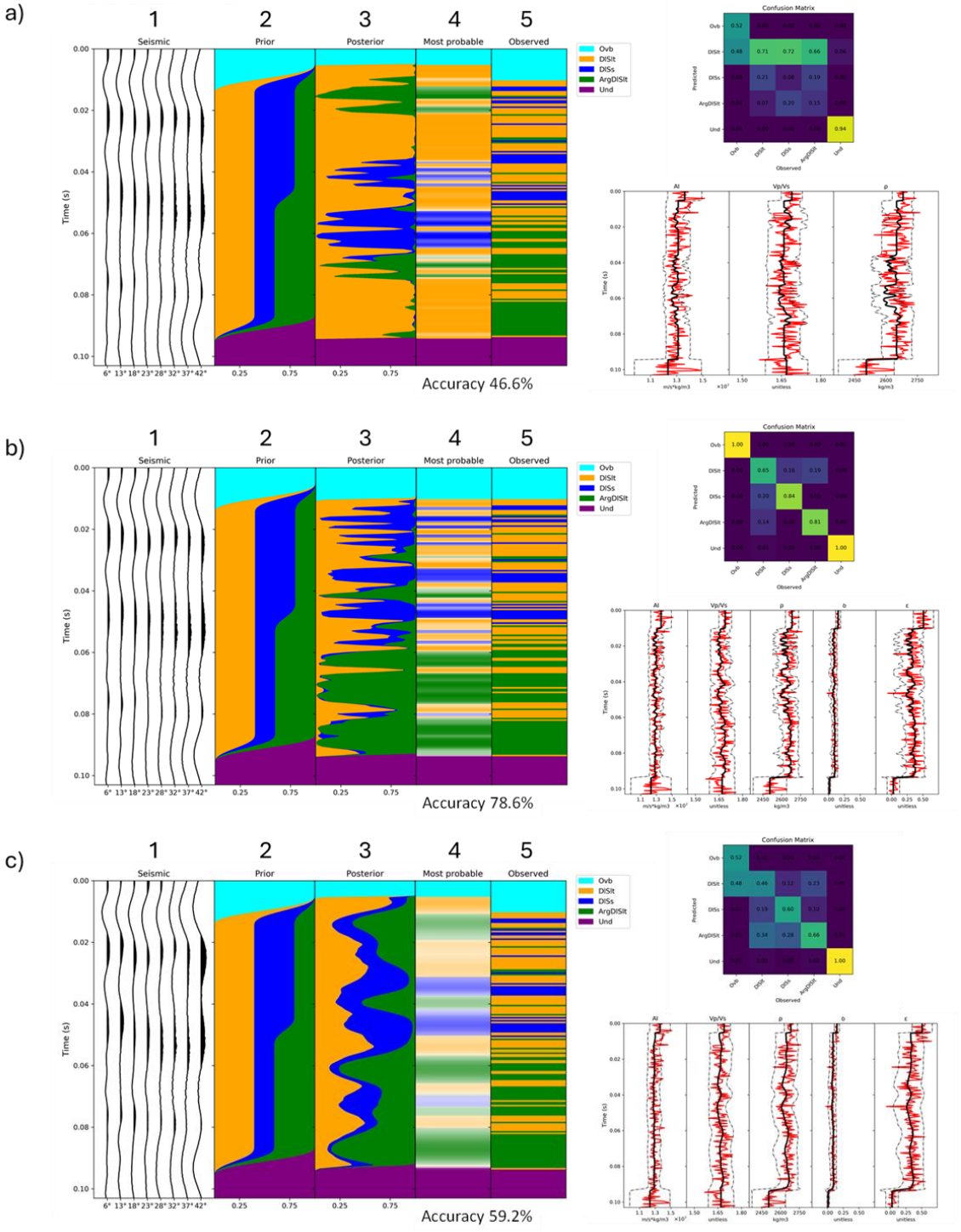

Figure 11: (a) Isotropic DPI with VTI synthetic gather input, with track 1 showing input synthetic gather traces, track 2 showing prior model colour-coded by facies, track 3 depicting posterior full probability range output result, and track 4 the most-probable facies panel and finally track 5 the observed log facies panel. The confusion matrix of the predicted posterior output (y-axis) vs the input observed facies (x-axis) for accuracy assessment is shown on the top right. To the bottom right are shown the log curves for AI, V_P/V_S and Rho elastic properties (red tracks) compared to output mean posterior elastic facies (black tracks) with grey tracks' depicting the bounds of two standard deviations.

(b) An equivalent set of images similar to those shown in (a) for VTI-DPI with VTI synthetic gather input and lower right log tracks that include Thomsen parameters d and e in addition to AI, V_P/V_S and Rho. (c) An equivalent set of images similar to those shown in (b) but generated to illustrate the impact of adding random noise to the input VTI synthetic gather traces. The addition of noise reduces the average accuracy, indicated on the log segments, as well as the confusion matrix.

affect the higher angle traces and not the zero angle traces as shown in the model AVO curves in Figure 3. By contrast the predicted V_P/V_S and ρ black overlay tracks do not match the red log tracks as these elastic properties are functions of the AVO gradient that are very sensitive to VTI effects.

Figure 11b shows the results of applying VTI DPI to a VTI input model. The inversion output is presented as posterior facies probabilities (track 3). Compared to the prior probabilities, the posterior probabilities contain more detailed stratigraphic information. Notably, the resolution of the inversion results is higher and well below the tuning thickness expected from the frequency content of the seismic data (mean frequency 45 Hz). More importantly, the VTI inversion results reflect the correct facies' proportions, i.e. an upper half dominated by dolomitic siltstones while the lower half is predominately made of argillaceous dolosiltstones with thicknesses increasing with depth.

A comparison of the results in Figure 11b to the isotopic inversion results shown in Figure 11a demonstrates that the posterior output probability range and the most probable facies more accurately resolve the observed facies as seen clearly in track 4, with a prediction accuracy improvement of 79%. Furthermore, the confusion matrix of predicted vs observed facies probabilities are now more aligned on the central 1:1 diagonal that reflects the overall 79% average accuracy improvement. Lastly, the bottom right log track overlays of the predicted black tracks for V_P/V_S and Rho are strongly correlated to the observed red log tracks as are the new additional VTI Thomsen parameter estimates for δ and ε.

Figure 11c shows the final example in this proof-of-concept VTI DPI test, demonstrating the impact of adding colored random noise to the input VTI synthetic gather traces to simulate more realistic seismic data. As expected, the addition of noise reduces the average prediction accuracy to 60% with a visible reduction in the confusion matrix, where the 1:1 diagonal indicating correct facies, prediction is noticeably less prominent. Further, the predicted posterior black track overlays for all elastic and VTI parameter estimates have a lower resolution with a poor smoother correlation with the observed red log tracks.

We can summarize some of the important observations from the above discussion as follows:

- DPI solves the seismic AVO inversion problem using Bayesian inference, enabling flexible interpretation strategies:
  - Probabilistic facies classification is available for P10, P50, and P90 models.
  - DPI allows the integration of geological information such as layer thicknesses and stratigraphic ordering, during inversion.
- DPI can resolve geological layers below tuning thickness.

- Dramatic improvements are observed in accuracy and resolution of inversion results.
- DPI is capable of distinguishing between facies with similar properties.
- VTI-DPI offers two additional elastic parameters (delta and epsilon) that improve facies classification results.
- Applying isotropic models to data that exhibit VTI anisotropy can lead to incorrect estimates of V_P/V_S and density.
- The presence of noise decreases the resolution of the VTI-DPI output. The magnitude of this effect is facies-dependent.

Inversion results on 3D seismic data – Montney case study

This section presents an example of integration, where information from standard processed seismic AVO data is integrated with information from a range of other domains from different domains such as well logs, seismic data and geology, as described above. This integrative approach demonstrates how QI for unconventional reservoir characterization can be significantly improved, particularly in the estimation of key rock physics (seismic petrophysics) parameters that influence hydraulic fracturing performance. These parameters include rock quality heterogeneity (e.g. mineralogical brittleness, porosity, kerogen-TOC), the presence of natural fractures and in-situ stress conditions.

The case study examples show how information from standard processed seismic AVO data is integrated with information from a range of other domains such as well logs, seismic data and geology, as described above. Specifically, the two field examples from the Montney Formation are presented, showcasing the advantages of Direct Probabilistic Inversion (DPI) in characterizing tight unconventional siltstone reservoirs. In both cases, DPI integrates geologic priors (facies thickness, stratigraphic order, transition probabilities) and outputs facies probability volumes, enabling detection of thin beds and facies transitions those conventional deterministic inversions struggle to resolve.

Montney Case 1 Low-resolution stratigraphic sequence

In a deep Montney interval with poor seismic resolution, even the top of the Montney is challenging to identify on conventional seismic data and deterministic elastic volumes. Applying DPI in this setting yielded an explicit stratigraphic layering of the Montney, revealing internal units that were previously difficult to interpret. Figure 12 represents the facies defined for the DPI framework (Figure 12a), where the transition matrix (Figure 12b) illustrates the probabilities of one given facies transitioning into the next. The high probabilities are geologically reasonable and will drive the inverted solution.

Figure 13 illustrates a comparison of the seismic stack (Figure 13a) and acoustic impedance results from the deterministic inversion (Figure 13b), and the DPI facies prior (Figure 13c) and posterior (Figure 13d) results for a Montney cross-section. with three well ties The DPI most-likely facies display (Figure 13d) clearly delineates stratigraphic boundaries and lithofacies, notably identifying a thin, porous siltstone sub-unit (yellow) in the middle Montney that is

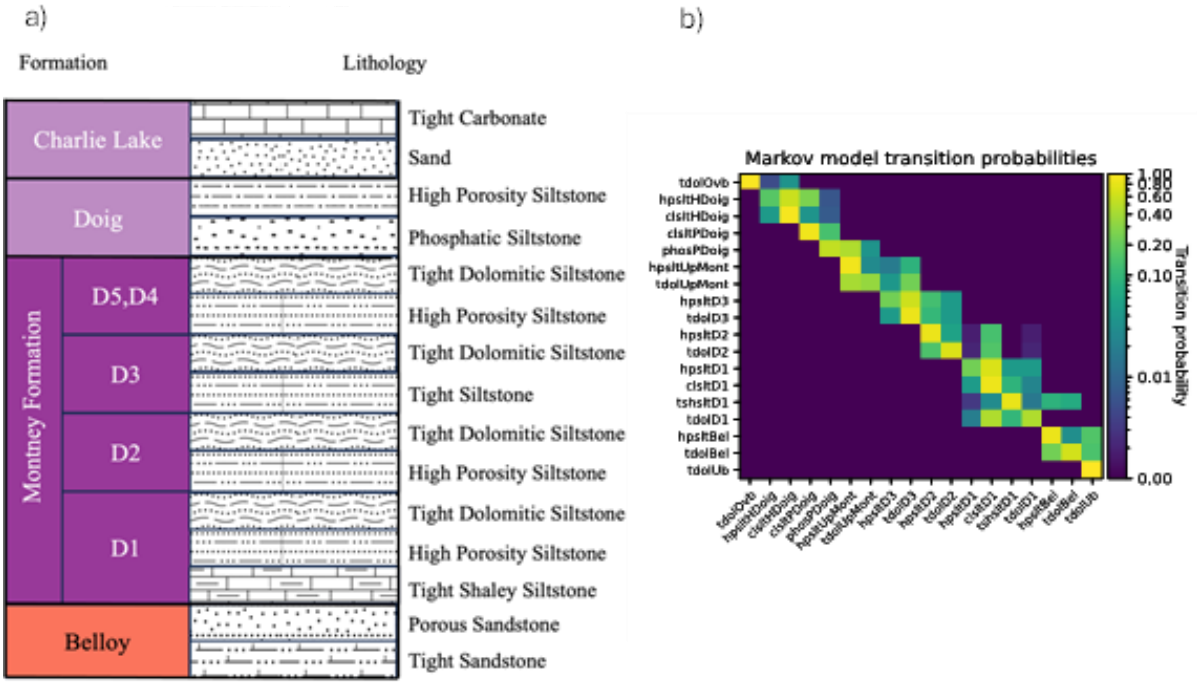

Figure12: (a) Facies definition, and (b) transition matrix, for DPI framework. (Mutual et al., 2024)

effectively invisible in the other volumes. This unit corresponds to the high porosity siltstone D4 unit in Figure 12a. This sub-seismic reservoir layer is a known target zone for horizontal wells; DPI's ability to resolve and map this zone provides a tangible benefit for geo-steering and well landing, as missing this layer by drilling out of zone can adversely affect well performance. The DPI result also deviated significantly from the initial model, which was built from sparse horizon picks, indicating that the inversion is not simply reproducing the prior but adding geological detail supported by the seismic. At two blind well locations, the DPI facies prediction showed a good match to observed facies logs, correctly identifying the placement and thickness of major porous siltstone beds (yellow facies) that the prior model had misrepresented. Moreover, DPI captured variations in overburden and intra-Montney unit thickness that were beyond seismic resolution and omitted in the prior, highlighting the value of the probabilistic approach in updating the stratigraphic model. This case demonstrates that by directly inverting for facies with a Bayesian framework, DPI can resolve thin beds and subtle facies changes below seismic tuning, providing a level of vertical resolution and stratigraphic clarity unattainable with deterministic methods.

Montney Case 2 Facies probability and stress characterization

The second case study integrates DPI into a broader quantitative interpretation workflow for the Montney Formation and is illustrated in Figure 14. Here, deterministic AVO inversion and rock physics inversion was first used to estimate elastic properties (AI, V_P/V_S, ρ) and rock properties (porosity, mineral fractions, etc.), which in turn fed a geomechanical model for minimum horizontal stress estimations. This deterministic approach provided an initial estimate of closure stress that aligned well with measured values, lending confidence to the seismic-derived

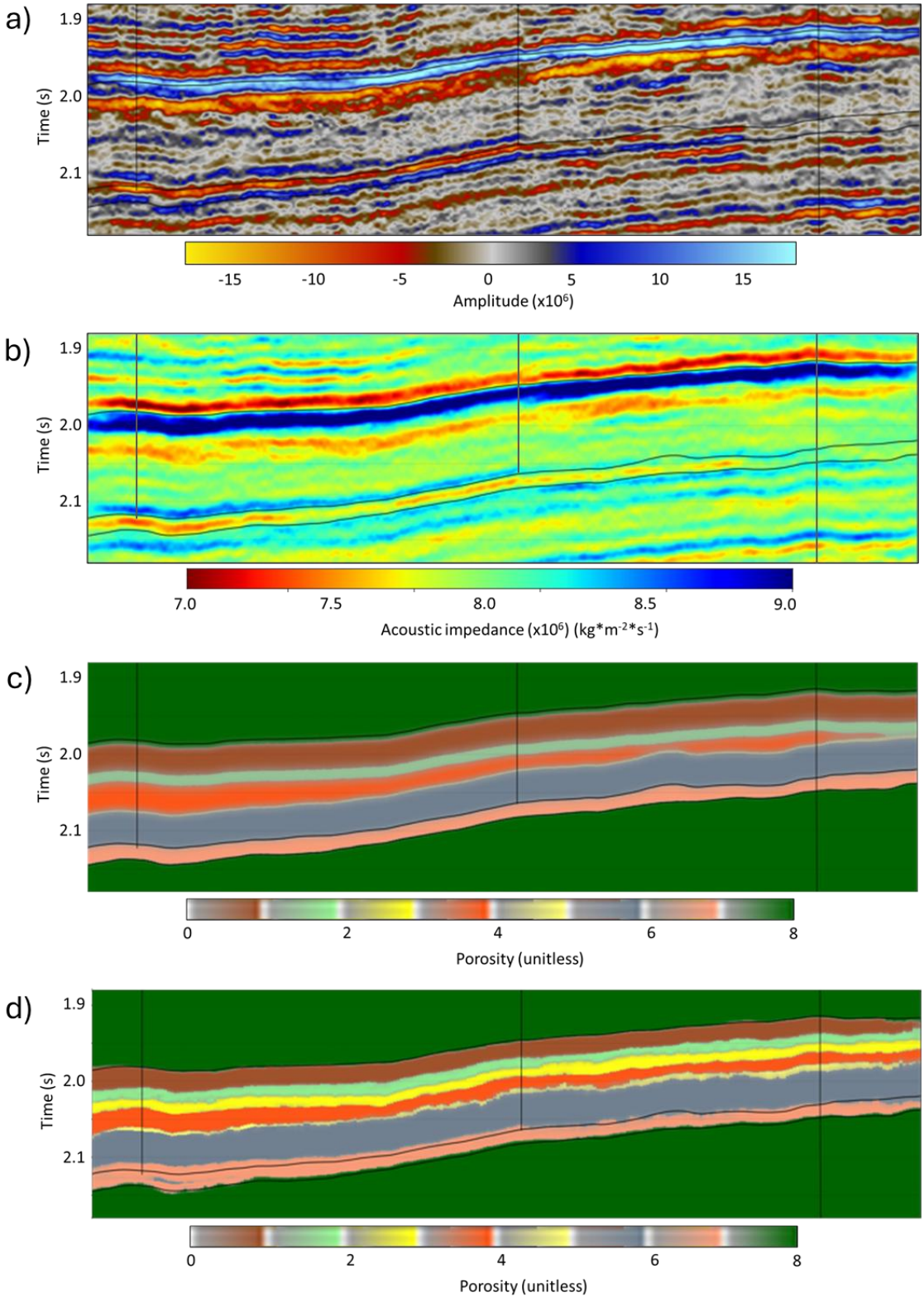

Figure 13: An arbitrary line passing through three wells and drawn from (a) seismic, (b) deterministic acoustic impedance, (c) DPI facies prior, and (d) DPI most likely facies. (Adapted from Mutual et al., 2024)

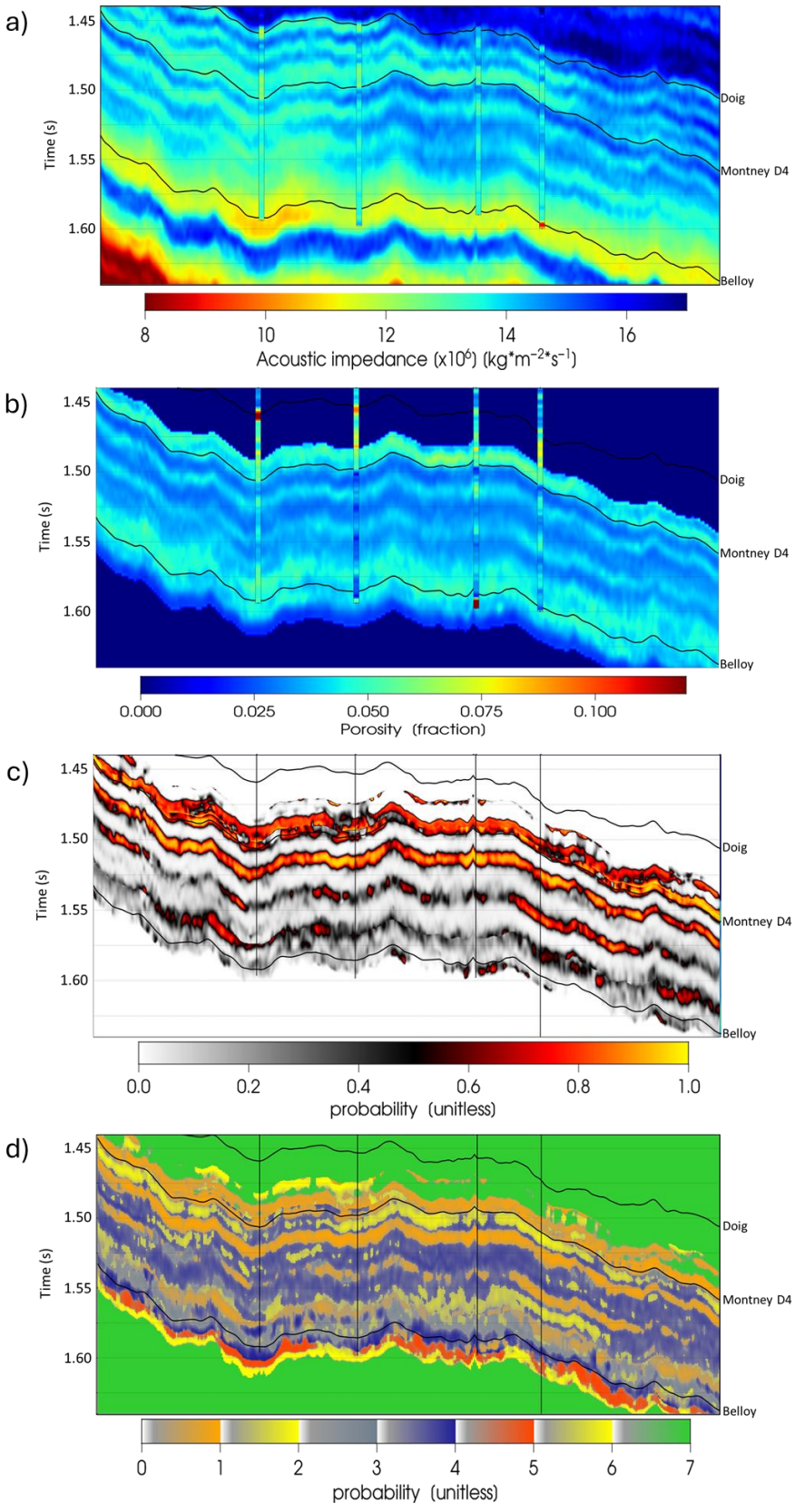

Figure 14: An arbitrary line passing through four wells and drawn from (a) acoustic impedance, (b) total porosity, (c) DPI porous siltstone, and (d) DPI most likely facies volumes. The DPI facies display exhibits much sharper stratigraphic detail and continuity which directly benefits reservoir characterization. (Adapted from Gordon et al., 2023)

predictions. DPI was then employed to directly invert the seismic for facies probabilities, using a prior model with these lithofacies:

- High-porosity siltstone
- Low-porosity (tight) siltstone
- Organic-rich siltstone
- Organic-rich dolomitic siltstone
- Porous sand
- Tight sand

These facies span the Upper, Middle, and Lower Montney members, capturing the vertical heterogeneity of the formation. The DPI results dramatically improved facies discrimination across the Montney compared to a traditional deterministic classification (Figure 14). For instance, in the Upper Montney, DPI assigns a high probability to porous siltstone facies, consistent with slightly elevated porosities seen in the rock physics (Figure 14b) inversion and with the known sweet spots in that interval. This is a notable improvement over the deterministic inversion, which was already used successfully to identify landing zones.

These results are confirmed by the 4 well penetrations.

Across the section (Figure 14d), the Upper Montney is clearly characterized by a dominance of porous siltstone (yellow-orange) with interbedded tight siltstone, whereas the Middle and Lower Montney are dominated by organic-rich siltstone facies (gray tones) with minor porous streaks. The DPI facies volume exhibits much sharper stratigraphic detail and continuity than the prior model (or any deterministic inversion output), while still honoring the overall trends. This increased resolution and accuracy directly benefit reservoir characterization: for example, identifying the extent of organic-rich zones vs. more porous intervals can guide completion strategies and explain production differences across the Montney. By providing a range of probable facies rather than a single deterministic estimation, DPI also allows uncertainty analysis (e.g. generating P10/P50/P90 facies models for risk assessment), although this was outside the scope of the case studies. Overall, DPI delivered significantly more detail in the most-probable facies model compared to deterministic methods, even though it also struggled in the lower Montney likely due to poor quality seismic.

Both case studies validate that incorporating DPI into Montney reservoir studies enhances the interpretation of thin stratigraphic units and heterogeneous lithologies. The results not only confirm known features (e.g. porous siltstone benches in the Upper Montney) but also reveal new sub-seismic facies architecture that can be critical for well planning and reservoir management.

In summary, DPI's integrated probabilistic approach provided a richer and more reliable characterization of the Montney Formation, improving facies prediction and supporting better-informed decisions for both hydrocarbon development and reservoir stimulation in these tight siltstone plays.

CONCLUSIONS

The direct probabilistic inversion (DPI) of both isotropic and anisotropic AVO data provides superior vertical resolution compared to a deterministic AVO inversion. This resolution advantage was observed in real 3D seismic testing. In synthetic tests, the incorporation of anisotropic effects enabled the inversion to correctly capture changes in the AVO gradient resulting from a change in V_P/V_S and/or shifts in the Thomsen VTI anisotropy parameters, δ and ε. This differentiation is not possible when using isotropic formulations in which the presence of anisotropy would result in an incorrect estimation of the gradient-related elastic parameters such as V_P/V_S, shear-impedance, density.

Since DPI outputs are probability estimates for each facies at different depths, a more comprehensive statistical analysis can be performed. Although not demonstrated in this paper, P10, P50 and P90 models can be derived for a more in-depth interpretation and exploration risk analysis.

Under reasonable assumptions, a high-dimensional Bayesian inference problem can be reduced to several local low-dimensional inference problems. This enables the application of a general and flexible probabilistic framework for rigorous propagation of uncertainties and for integrating prior knowledge from multiple domains. Moreover, this approach makes the Bayesian inversion a computationally affordable solution for large-scale industry AVO seismic datasets. The results of this study illustrate the ability of this method to provide probabilistic volumes of lithofacies (sand, shale variability, carbonate…), fractures and effective porosity, kerogen and fluids in non-equant porosity and horizontal stress anisotropy due to tectonic stresses for anisotropic elastic parameters that overprint isotropic estimates, at, and below, seismic tuning due to the utilization of statistical prior information.

REFERENCES

Aki K., and Richards P.G., 1979, Quantitative Seismology, W. H. Freeman & Co.

Blangy, J. P., 1994, AVO in transversely isotropic media- An overview, Geophysics, **59**(5), 775-781. https://doi.org/10.1190/1.1443635

Buland, A. and H. Omre, 2003, Bayesian linearized AVO inversion, Geophysics, **68**(1), 185-198. https://doi.org/10.1190/1.1543206

Goodway W., 2001 AVO and Lamé constants for rock parameterization and fluid detection, CSEG Recorder, **26**, Special issue.

Goodway, B., J. Varsek, and C. Abaco, 2006, Practical applications of P-wave AVO for unconventional gas Resource Plays: Part 1. CSEG Recorder Special Edition, **31**, 90-95.

Goodway, B., J. Varsek, and C. Abaco, 2006, Practical applications of P-wave AVO for unconventional gas resource plays: Part 2, CSEG Recorder, **31**, 52-64.

Goodway B., M. Perez, J. Varsek, and C. Abaco, 2010, Methods of seismic petrophysics and isotropic-anisotropic AVO for unconventional gas exploration, The Leading Edge, **29**(12), 1500-1508. https://doi.org/10.1190/1.3525367

Goodway B., R. Cova, E. Mutual, A. Mills, A. Gordon, W. Pardasie, M. Perez, A. Iverson, 2021, Direct Probabilistic Anisotropic AVO Inversion to correctly populate Geomechanical model uncertainty in shales and tight reservoirs, CSEG Symposium Abstracts.

Gordon, A., R. Cova, E. Mutual, B. Goodway, S. Leaney, W. Pardasie, and M. Ng, 2023, Latin American Unconventional Resources Technology Conference, 207-212. https://doi.org/10.15530/urtec-2023-3971329

Grigg M., 2004, Emphasis on mineralogy and basin stress for gas shale exploration: Gas Shale Technology Exchange SPE meeting.

Hansen, H. J., A. F. Jakobsen, A. Jollands, and F. Nicholson, 2018, Local probabilistic inversion of seismic AVO data 80th EAGE Annual Conference, AbstractWS02. https://doi.org/10.3997/2214-4609.201801888

Jullum, M., O. Kolbjørnsen, 2016, A Gaussian-based framework for local Bayesian inversion of geophysical data to rock properties, Geophysics **81**(3), R75-R87. https://doi.org/10.1190/geo2015-0314.1

Larsen, A. L., M. Ulvmoen, H. Omre, and A. Buland, 2006, Bayesian lithology/fluid prediction and simulation on the basis of a Markov-chain prior model, Geophysics, **71**(5), R69–R78. https://doi.org/10.1190/1.2245469

Leaney S., 1994 AVO and anisotropy from logs and walkaways, Schlumberger Interpretation Development Forum, Jakarta, 623-630. https://doi.org/10.1071/EG993623

Leaney, S., and C. Sayers, 2024, Anisotropic priors for probabilistic AVA inversion, GeoConvention.

Mutual, E., I. Berezina, A. Jakobsen, B. Goodway, W. Pardasie, B. Riopel, and S. Hansen, 2024a, Probabilistic inversion for interpretation of a stratigraphic sequence in a poorly resolved unconventional reservoir, 4th IMAGE Meeting, Expanded Abstracts, 1652-1655. https://doi.org/10.1190/image2024-4093524.1

Mutual, E., A. Gordon, B. Goodway, R. Cova, S. Leaney, and W. Pardasie, 2024b, Reservoir characterization of various formations: probabilistic inversion approach, 4th IMAGE Meeting, Expanded Abstracts, 75-78. https://doi.org/10.1190/image2024-4101160.1

Perez, M., 2010, Beyond isotropy-Part I: A prestack perspective, CSEG RECORDER, **35**, 36-41.

Perez, M., 2010, Beyond isotropy-Part II: Physical models in LMR space, CSEG RECORDER, **35**, 36-43.

Perez, M., 2013, Seismic modelling of unconventional reservoirs, CSEG RECORDER, **38**, 62-70.

Perez, M., 2015, Extending LMR for anisotropic unconventional reservoirs, GeoConvention Abstracts, 1-4.

Rüger A., 1997, P-wave reflection coefficients for transversely isotropic models with vertical and horizontal axis of symmetry, Geophysics,**62**(3), 713-722. https://doi.org/10.1190/1.1444181

Sayers, C. M.,2004, Seismic anisotropy of shales: What determines the sign of Thomsen's delta parameter? Ann. Int. Mtg., SEG. Expanded Abstracts, Denver Colorado, 103-106. https://doi.org/10.1190/1.1845094

Tarantola, A.,2005, Inverse problem theory and methods for model parameter estimation, Society for Industrial and Applied Mathematics (SIAM).

Thomsen, L.,1986, Weak elastic anisotropy, Geophysics, **51**(10), 1954-1966. https://doi.org/10.1190/1.1442051

About the Authors

Bill Goodway *obtained a B.Sc. in Geology from University College London and a M.Sc. in geophysics from University of Calgary. After working in the UK, he joined PanCanadian Petroleum in 1985, becoming Team Lead of a Seismic Analysis Group and Advisor for Seismic Analysis at Encana. In 2010 he became Manager Geophysics-Advisor Senior Staff at Apache, involved in seismic acquisition design, processing interaction, experimental special projects and new AVO methods. Bill is currently Qeye's Scientific Advisor Quantitative Interpretation and AVO technology.*

Bill has authored numerous papers at CSEG, EAGE and SEG conventions on seismic acquisition design, processing, borehole geophysics, anisotropy, multicomponent recording and QI/AVO.

He was awarded four CSEG Best Paper Awards, the CSEG Medal and was a past SEG Honorary Lecturer for North America. The CSEG recognized Bill as the 2013 Symposium honouree and in 2016 he received the SEG's Reginald Fessenden Award for lambda-rho-mu (LMR) inversion technology.

Raul Cova *received his B.Sc. Degree in geophysics in 2004 from Simon Bolivar University in Venezuela. Between 2004 and 2012, he worked for PDVSA, occupying roles related to seismic data acquisition, processing, and interpretation. He obtained his Ph.D. degree at the University of Calgary in 2017, where he was a fellow of the CREWES consortium. He continued at the University of Calgary as a postdoctoral researcher working on full-waveform inversion problems. Raul joined Qeye Labs in Calgary in 2019, where he is now a Team Lead specializing in AVO inversion and advanced reservoir characterization techniques.*

Evan Mutual *has over ten years of related work experience in advanced seismic and rock physics analysis. He has worked with on-shore and off-shore seismic data from around the world in a wide array of geologic settings. He helped establish the Qeye Calgary office and helped it grow from 2 people to over 10. Through his work he has helped develop workflows for effective stress characterization, anisotropy analysis, joint inversions and most recently a workflow for the integration of seismic data and reservoir model or geomodel data.*

Adriana Gordon *is a QI geophysicist. She earned a B.Sc. in geophysical engineering from Simón Bolívar University (2015) and an M.Sc. in geophysics from the University of Calgary (2019), where—working with CREWES—she advanced DAS and geophone VSP data processing for CO_2 storage and monitoring in southern Alberta. Since 2019, Adriana has led AVO-inversion projects at Qeye across North and South America, applying full-cycle seismic-inversion workflows spanning data conditioning, simultaneous AVO inversion, rock-physics modeling, and 4D analysis.*

To deepen her data-science toolkit, she is completing a second master's in analytics at the Georgia Institute of Technology.

Irina Berezina *earned a B.Sc. in geology from Lomonosov State University in Russia in 2010, followed by an M.Sc. in geophysics from the same institution in 2012. In 2023, she joined Qeye Labs as a QI Geophysicist. Prior to her role at Qeye, she worked as a research fellow at the Schmidt Institute of Physics of the Earth from 2013. Irina has experience in rock physics and quantitative interpretation.*

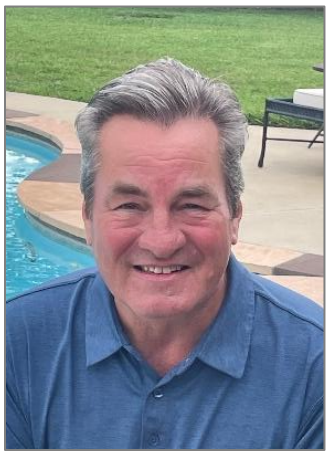

Scott Leaney *has M.Sc. and Ph.D. degrees from the University of British Columbia and a B.Sc. from the University of Manitoba, all in geophysics. He worked internationally for Schlumberger for 32 years, beginning in 1988 in France, in engineering, followed by positions in operations and R&D (Indonesia, Japan, England, Houston). These days he works from his consultancy (SLRDC) and has been consulting part-time for Qeye since 2022, focusing on anisotropic model building from logs and inversion in anisotropic media. He has numerous publications and holds six sole inventor patents, was awarded the 1986 SEG Best Student Paper, 1999 EAGE Distinguished Lecturer and 2015 Geoconvention Best Paper. His hobbies include golf and the physics of curling.*